
Article:
Parry, J.A., Horoshenkov, K.V. and Williams, D.P. (2020) Pressure ratio and phase difference in a two-microphone system under uncertain outdoor sound propagation conditions. Applied Acoustics, 170. 107548. ISSN: 0003-682X

https://doi.org/10.1016/j.apacoust.2020.107548

Pressure ratio and phase difference in a two-microphone system under uncertain outdoor sound propagation conditions

Jordan A Parry[1], Kirill V Horoshenkov[1], Duncan P Williams[2]
[1]University of Sheffield, Dept. of Mech Engineering, Sheffield, England
JAParry1@Sheffield.ac.uk; K.Horoshenkov@Sheffield.ac.uk;
[2]Defence Science and Technology Laboratory, Salisbury, England
DPWilliams@dstl.gov.uk;

Abstract

Predictions of outdoor sound propagation in uncertain conditions is a challenging task. Evidence suggest that using more than one receiver can reduce this effect of uncertainties. This paper studies via numerical simulations the effects of uncertainty in the source/receiver geometry and impedance ground condition on the sound pressure ratio recorded using the two-microphone method. A Monte Carlo method is employed study the effect of uncertainties in the range and ground parameters. The range and frequency are found to be key parameters which control the resultant probability density function for the absolute sound pressure ratio and phase difference. The introduction of small uncertainty only matters if the uncertainty is present in the distance between the source and receiver. Uncertainties in the impedance ground are found to have a negligible effect. The sound pressure ratio is affected by the uncertainty more strongly at a shorter range. These findings pave the way to the development of more robust methods for outdoor acoustic source localisation and identification from two-microphone data.

1. Introduction

The two-microphone method is used extensively in outdoor sound propagation to determine the ground impedance from the acoustical data (e.g. [1]), noise control (e.g. [2]) and source localisation (e.g. [3]). American National Standards Institute (ANSI) provides a standard method for determining the acoustic impedance of ground surfaces using the ratio between two close microphones to infer an impedance of an unknown ground using carefully obtained acoustical data [4]. The use of a sound pressure ratio or level difference between the two microphones cancels out troublesome interference patterns and source spectrum effect, allowing for more accurate predictions of the ground properties and environmental effects.

A key for the successful use of this method is the quality of the sound pressure measurements and microphone mismatch. While Harriot and Hothersall investigated the accuracy of the signal processing method in the presence of an uncertain ground, especially the interference patterns, the geometric and frequency ranges used in this standard are far too small to study whether these effects carried over into the larger geometries and/or more varied sound sources [5]. Kruse and Mellert [6] used the two-microphone method to measure errors from uncertainties present in outdoor sound propagation over a wider frequency range. Errors were minimised at frequencies above $100Hz$ and $500Hz$ for acoustical soft and hard impedance grounds respectively, yet the study did not investigate the medium/longer ranges (>100 m) which are of common interest in outdoor acoustics and there is a limited statistical data on the sound pressure ratio and phase mismatch.

This study aims to increase the scale of the geometries used and assess the viability of the two-microphone method for the statistical analysis of outdoor sound propagation. One effect which has not been quantified yet, is the influence on geometrical uncertainties on the probabilistic measures of the sound pressure data obtained on a pair of microphones. A main research question here is: *How does the uncertainty in the sound/receiver position affect the absolute sound pressure ratio and phase*

difference between the two microphones used with this method? These parameters are important in the understanding of outdoor sound propagation, with specific application to the inverse problems such as sources localisation, identification and ground property inversion. Other questions are also answered in the study, such as whether the two-microphone method is applicable for large scale studies and the computational efficiency that can be achieved with readily available hardware, having possible direct impact on the analysis of outdoor sound propagation methods used by the industry and academia.

This paper is structured in the following manner. Section 2.1 details the acoustical methods, such as the acoustical model and the physical representations of gathered outputs. Section 2.2. outlines the statistical methods applied to study the uncertainty. Section 3 presents and reviews the results from our simulations. Finally, Section 4 summarises the main findings of this study.

2. Research Methods

2.1. The model

This study makes three key initial assumptions about the acoustical scenario: (i) non-moving homogenous atmosphere; (ii) a 2D (r, z) problem geometry with a point source; and (iii) a homogeneous impedance ground with well-defined acoustical characteristics between the source and receivers. The first assumption is used to understand the geometrical uncertainty in the absence of atmospheric effects. The 2D geometry is not a concern because it is used extensively and successfully for outdoor sound propagation modelling (e.g. [4]). The final assumption of the uniform ground is acceptable because prior works have shown that a relatively large variability in the ground does not significantly affect the interaction paths over the scales adopted in this study [7].

The American National Standard S1.18 method for determining an acoustic impedance of a ground [4] inspired this work. The ANSI S1.18 standard makes used of the ratio and corresponding level difference between the sound pressures obtained on two closely spaced receivers installed at the same range (r) from the point source. These two receivers are installed at two distinct receiver heights (h_r). This study uses the recorded pressure, and the ratios between these measures, at the receivers to establish; (i) the absolute pressure ratio and (ii) phase difference.

To calculate these values, it is first recounted that the sound pressure measured at a receiver from a source [8] can be equated to be

$$p = p_0[1 + Q\frac{R_1}{R_2}\exp\big(ik(R_2 - R_1)\big)] \ , \tag{1}$$

using the time convention $\exp(-j\omega t)$, where $p_o,\ k$ and Q are the reference sound pressure at 1 m from the source, wavenumber and spherical wave reflection coefficient, respectively. The distances R_1 and R_2 can be defined as

$$R_1 = \sqrt{r^2 + (z - z_s)^2} \, , \tag{2}$$

$$R_2 = \sqrt{r^2 + (z + z_s)^2} \, , \tag{3}$$

for given source (z_s) and the receiver (z) heights, respectively. R_1 and R_2 represents the directed and reflected path respectively. The spherical wave reflection coefficient (Q) accounts for the effect of the locally reactive impedance ground on the reflected rays. The equation for the spherical wave reflection coefficient is

$$Q = \left(\frac{Z\cos\theta - 1}{Z\cos\theta + 1}\right) + \left(1 - \left(\frac{Z\cos\theta - 1}{Z\cos\theta + 1}\right)\right) F(w)\,. \tag{4}$$

The angle θ is the incident angle at which the reflected ray leaves the impedance ground, given as θ_A and θ_B in Fig. 1 for the different paths to each respective receiver. The function $F(w)$ accounts for the boundary loss factor and it is defined as

$$F(w) = 1 + iw\sqrt{\pi}\exp(-w^2)\,\mathrm{erfc}(-iw)\,, \tag{8}$$

with $\mathrm{erfc}(-iw)$ being the complimentary error function

$$\mathrm{erfc}(z) = \frac{2}{\sqrt{\pi}}\int_z^{\infty}\exp(-t^2)\,dt\,. \tag{9}$$

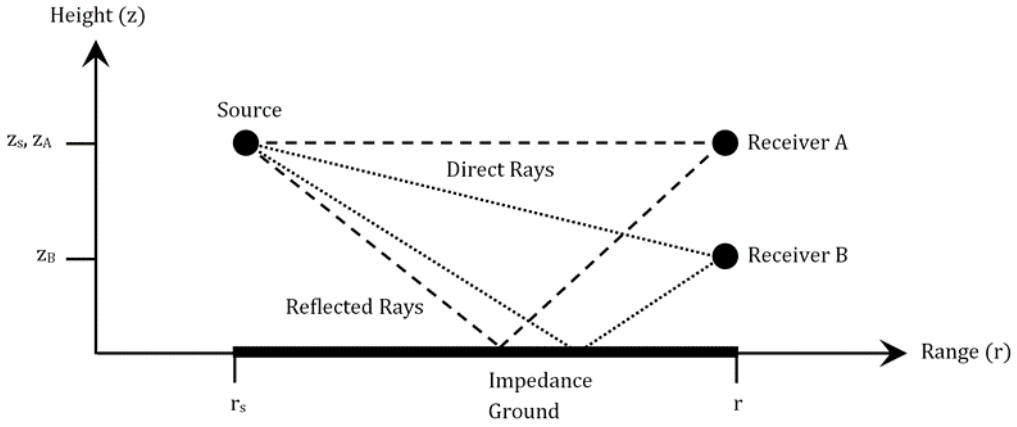

Figure 1: Acoustic scenario of the two-microphone system in the (r, z) geometry.

The parameter Z in eq. (4) is the normalised impedance of the ground, which is dependent on the acoustic properties of said ground. The impedance Z is determined using the model proposed by Horoshenkov et al [9]. This model calculates the acoustic properties of the impedance ground by considering the ground as a porous media with pores of non-uniform cross-section, with the median pore-size $\bar{s}$.

In outdoor sound propagation studies, it is common to refer to the effective flow resistivity of the ground (σ_g). The acoustic impedance model proposed in [9] relates the effective flow resistivity to the median pore size as

$$\sigma_g = \frac{8\eta\alpha_\infty}{\bar{s}^2\phi}e^{6(\sigma_s\log 2)^2}\,, \tag{10}$$

where η is the dynamic viscosity of air. In the above equation it is common to set the values of porosity (ϕ) and tortuosity (α_∞) to unity and standard deviation in pore size (σ_s) to zero, because for a majority of outdoor ground types their influence on the value of effective flow resistivity is relatively small in comparison with that of the median pore size. This value will be used to determine the grounds effect on the interaction patterns between reflected and direct sound rays.

The sound pressure at the receiver positions A and B is

$$p_A = p_0[1 + Q\frac{R_{1A}}{R_{2A}}\exp\big(ik(R_{2A} - R_{1A})\big)]\,, \tag{11}$$

$$p_B = p_0[1 + Q\frac{R_{1B}}{R_{2B}}\exp\big(ik(R_{2B} - R_{1B})\big)]\,, \tag{12}$$

where the distances are now dependent on the direct paths to the receivers A and B (R_{1A} & R_{1B}) and reflected from the ground paths (R_{2A} & R_{2B}). Using eq. (10) and eq. (11), the sound pressure ratio between the signals recorded on receiver A and B is

$$p_d = \frac{p_A}{p_B}\exp(i\phi_B - i\phi_A)\,. \tag{13}$$

Two parameters in eq. (13) are of direct interest: (i) the ratio of the sound pressure amplitudes, $\mu_p = \frac{p_A}{p_B}$; and (ii) the phase difference, $\mu_\phi = \phi_B - \phi_A$. The uncertainty in the sound pressure amplitude ratio can alter the quality of the ground impedance inversion method [4], whereas the uncertainty in the phase difference would affect the accuracy of source localisation [3].

2.2. Propagation of Uncertainty

The problem approached in this work is of a forward nature, where the uncertainty is added into the model, which we assume to be perfect i.e. the model would predict the exact result for a given set of parameters. It is assumed that there is a variability in the geometry and ground properties, specifically in: (i) the range (r); and (ii) the ground impedance which is controlled by the effective flow resistivity (σ_g). The heights of the source (z_s), receiver A (z_A) and receiver B (z_B) are assumed locked to $1.5m$, $1.5m$ and $0.5m$, respectively. The range (r) is varied from $100m$ to $500m$, while the effective flow resistivity of the impedance ground takes the values of $100\mathrm{kPasm}^{-2}$ and $2000\mathrm{kPasm}^{-2}$. These values for the impedance follow some published experimental data [10] that corresponds to acoustical soft (e.g. grassland) and hard grounds (rocks), respectively.

For these ground types the real and imaginary parts of the sound pressure spectra at receiver A for $p_0 = 1$ Pa are illustrated in Fig. 2, which shows the real ((a) and (c) of Fig. 2) and imaginary ((b) and (d) of Fig. 2) parts of these spectra for a set of ranges. It is seen that the true spectra are all dependent on combinations of frequency (ω) and range (r) with visible differences between simulated results.

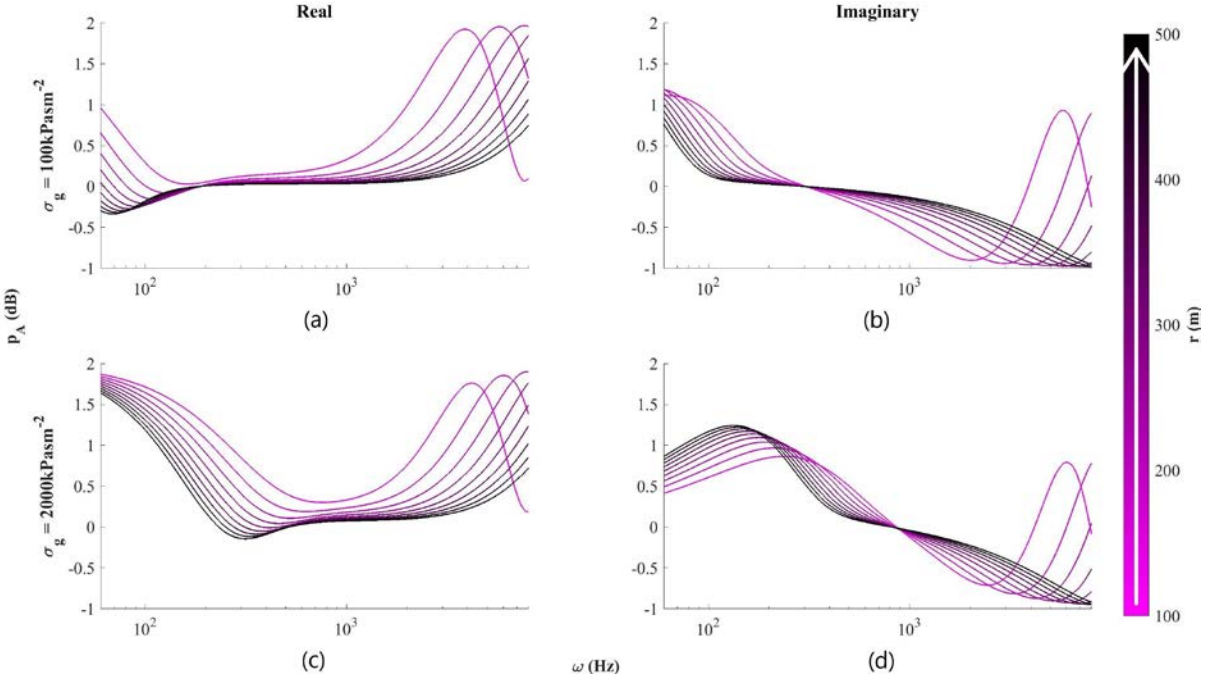

Figure 2: Real (Left column) and Imaginary (Right column) parts of the sound pressure predicted at position A as a function of the range. Top and bottom rows show data for acoustically soft $(100kPasm^{-2})$ and hard $(2000kPasm^{-2})$ impedance grounds, respectively.

In this paper the sensitivity in the model to some uncertainty in the range (r) and effective flow resistivity of the ground (σ_g) is studied through a Monte Carlo simulation. The Monte Carlo method is sampling method, that repeatedly calculates a given value while allowing for uncertainty to be present in certain model input parameters. In this case, the model employed is the one previously defined in eq. (13), predicting the sound pressure amplitude ratio and phase difference between the two receiver points.

The input parameters of the effective flow resistivity (σ_g) and range (r) are independently, and in combination, doped with uncertainty. This is done by replacing the true singular value, with a parameter randomly sampled from the given distribution. The given distributions used in this study are uniform distributions, which are flat distributions around the true value, meaning that any value inside the distribution is equally likely to be selected before each run of the Monte Carlo simulation. The uncertainty is controlled by changing how wide the distribution is i.e. lower and upper bounds being proportionally within either 5% or 35% of the true value.

This process is repeated for 1000 runs, for each combination of uncertainties, where for ease of analysis the average of each simulation is taken giving us the average sound pressure amplitude ratio $(\overline{\mu_p})$ and average phase difference $(\overline{\mu_\phi})$ in the frequency range of 60 Hz to 8 kHz. These parameters are the main focus of the analysis presented in the following section. The analysis is carried out visually and statistically, where kernel density estimation is used to generate the probability density functions (PDFs) of the average sound pressure amplitude ratio $(\overline{\mu_p})$ and average phase difference $(\overline{\mu_\phi})$.

3. Results

3.1. Sound pressure amplitude ratio

Fig. 3 shows the spectra of the average sound pressure amplitude ratios predicted for sound propagation in the presence of a relatively soft ground. Four situations are considered: (i) the fixed values of the parameters $(\sigma_g|r)$; (ii) uncertain value of the effective flow resistivity $(\Delta\sigma_g|r)$; (iii) uncertain value of the range $(\sigma_g|\Delta r)$; and (iv) uncertain values of the effective flow resistivity and range $(\Delta\sigma_g|\Delta r)$. Here Δ stands for the parameter uncertainty. Two sets of results are presented: (i) for $\Delta = 5\%$ of the given true value ((a), (b), (c) and (d) of Fig. 3); and (ii) for $\Delta = 35\%$ of the given true value ((e), (f), (g) and (h) of Fig. 3). Fig. 4 presents a similar set of results for the case of hard ground. Fig. 5 and Fig. 6 present the probability density functions for the average sound pressure amplitude ratios taken over the whole frequency spectrum. These are shown for each of the given combinations of parameter uncertainties.

The results from the Monte Carlo simulation suggest that the effect to the average pressure amplitude ratio $(\overline{\mu_p})$ for any combination of small uncertainties $(\Delta = 5\%)$ is relatively small, i.e. that this ratio predicted for these microphone locations is relatively immune to variations in the true value of range or flow resistivity of the ground. The effect of frequency on this ratio is dominant as suggested in ref. [3]. Visually, the spectra only show discernible differences from the true spectra ((a) and € in Fig. 4) when the true range (r) is less than $\leq 150m$ and large uncertainty $(\Delta = 35\%)$ is added to it ((d) and (h) in Fig. 4).

Statistically (See Table 1 in Appendix A) the mean of the average ratio of the sound pressure amplitudes $(\overline{\mu_p})$ increases from ~ 1.7 to ~ 2.9 as the range (r) increases. There is variation of ± 0.01 between the means for each hardness of the impedance ground which is controlled by the effective flow resistivity (σ_g). The standard deviation of the average ratio of the sound pressure amplitudes

$(\overline{\mu_p})$ decreases in line with the increase in range (r), with the deviation proportionally decreasing by 50% in the decrease from $500m$ to $100m$.

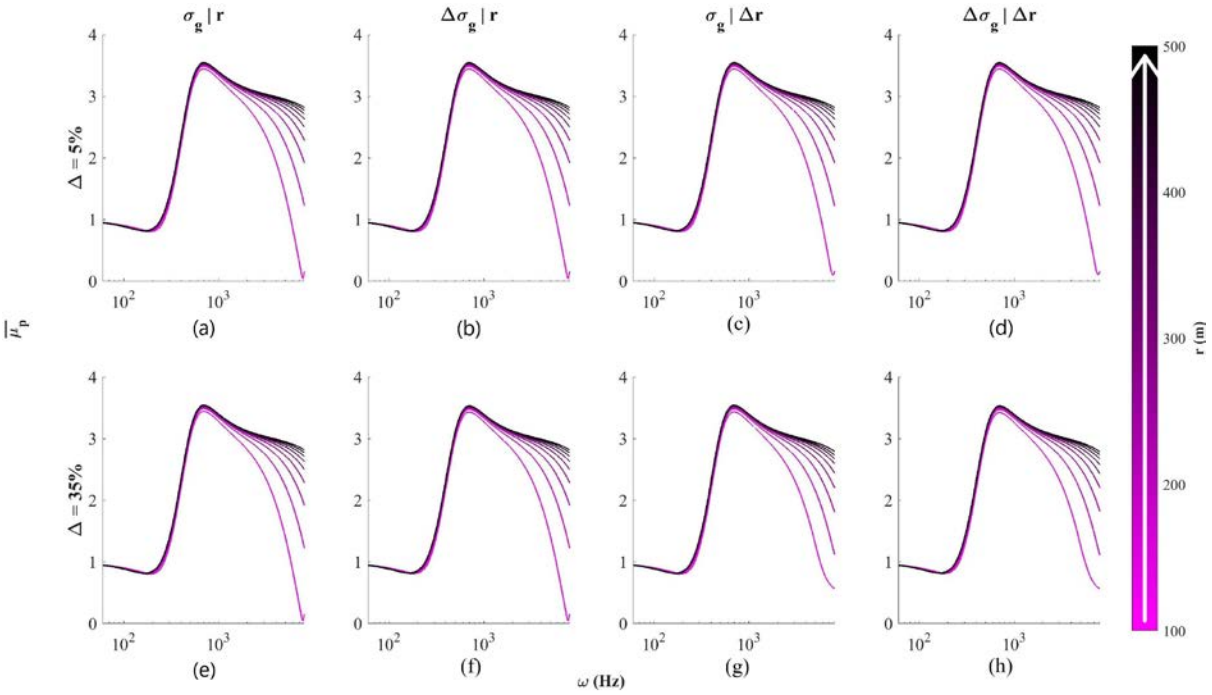

Figure 3: Simulation results for the average ratio of the sound pressure amplitudes $(\overline{\mu_p})$, for an acoustically soft ground $(\sigma_g = 100\text{kPasm}^{-2})$, where each column defining the uncertainty present and range (r) is mapped to colour, from magenta $(100m)$ to black $(500m)$. Uncertainty (Δ) is at 5% in the first row and increased to 35% in the second row.

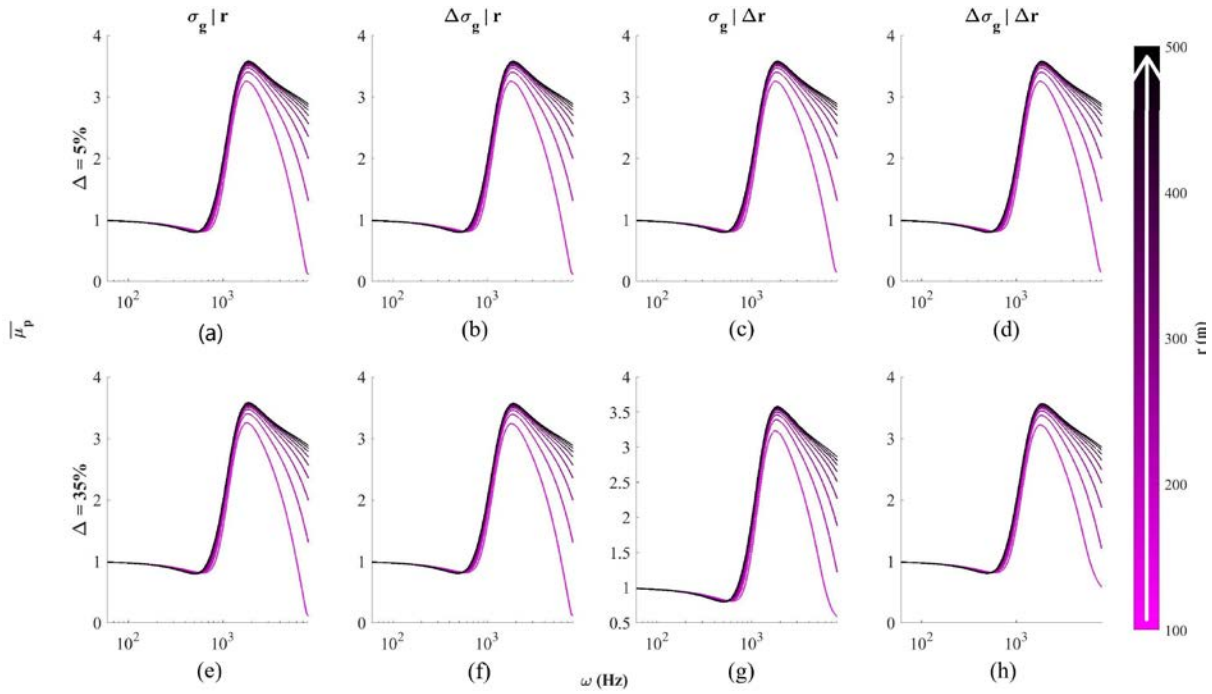

Figure 4: Simulation results for the average ratio of the sound pressure amplitudes $(\overline{\mu_p})$, for an acoustically hard ground $(\sigma_g = 2000\text{kPasm}^{-2})$, where each column defining the uncertainty present and range (r) is mapped to colour, from magenta $(100m)$ to black $(500m)$. Uncertainty (Δ) is at 5% in the first row and increased to 35% in the second row.

The generated PDFs seen in Fig. 5 and Fig. 6, for soft impedance $\left(\sigma_g = 100kPasm^{-2}\right)$ and hard impedance $\left(\sigma_g = 2000kPasm^{-2}\right)$ grounds respectively, allow for better insight into the effect of the uncertainty and range. Range (r) is the strongest parameter for shaping these distributions, creating a strong peak at $\overline{\mu_p}\sim 3$. This peak is reduced and disappears as the range reduces from $500m$ to $100m$ resulting in a close to flat distribution (see the magenta distributions in Fig. 5 and Fig. 6).

The strength of the peak is reduced for all simulations with the acoustical hardening of the impedance ground is increased i.e. an increase in flow resistivity $\left(\sigma_g\right)$. In this case the shape of the distribution and probability of other values (i.e. less than 3) do not change significantly. For the larger uncertainty $(\Delta = 35\%)$ and at the shortest range (e.g. $r = 100m$) another peak appears in the PDFs at $\overline{\mu_p}\sim 1$ (see Fig. 6).

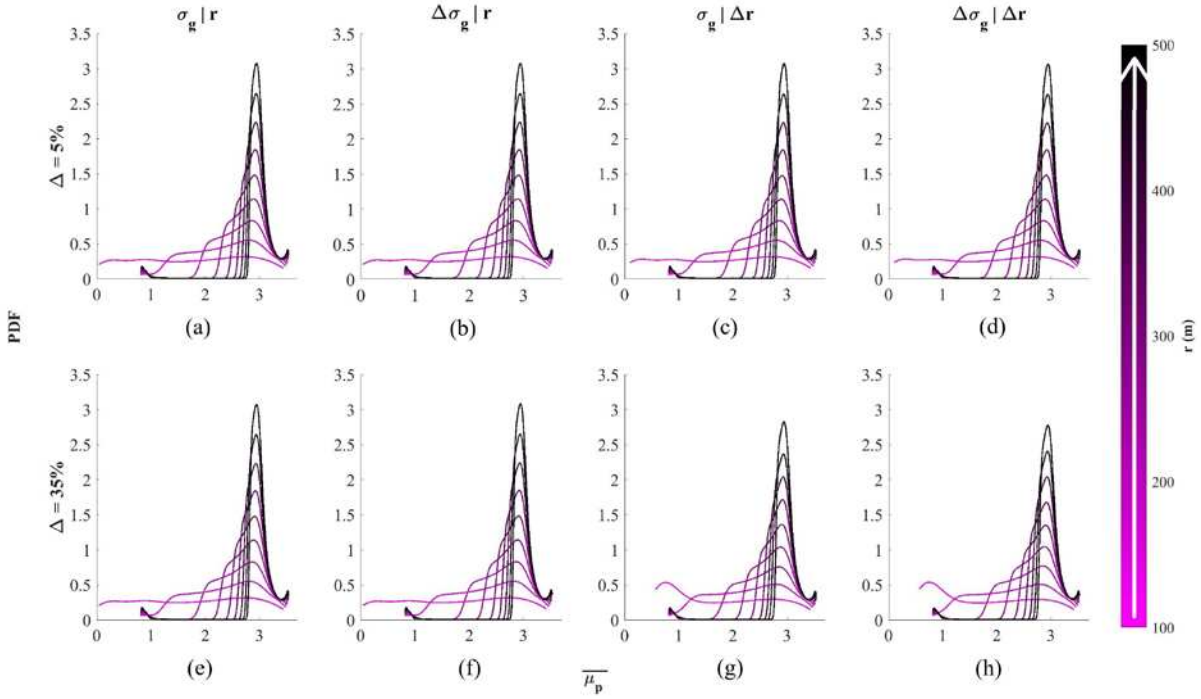

Figure 5: PDFs for the average ratio of the sound pressure amplitudes $\left(\overline{\mu_p}\right)$, for an acoustically soft ground $\left(\sigma_g = 100\text{kPasm}^{-2}\right)$, where each column defining the uncertainty present and range (r) is mapped to colour, from magenta $(100m)$ to black $(500m)$. Uncertainty (Δ) is at 5% in the first row and increased to 35% in the second row.

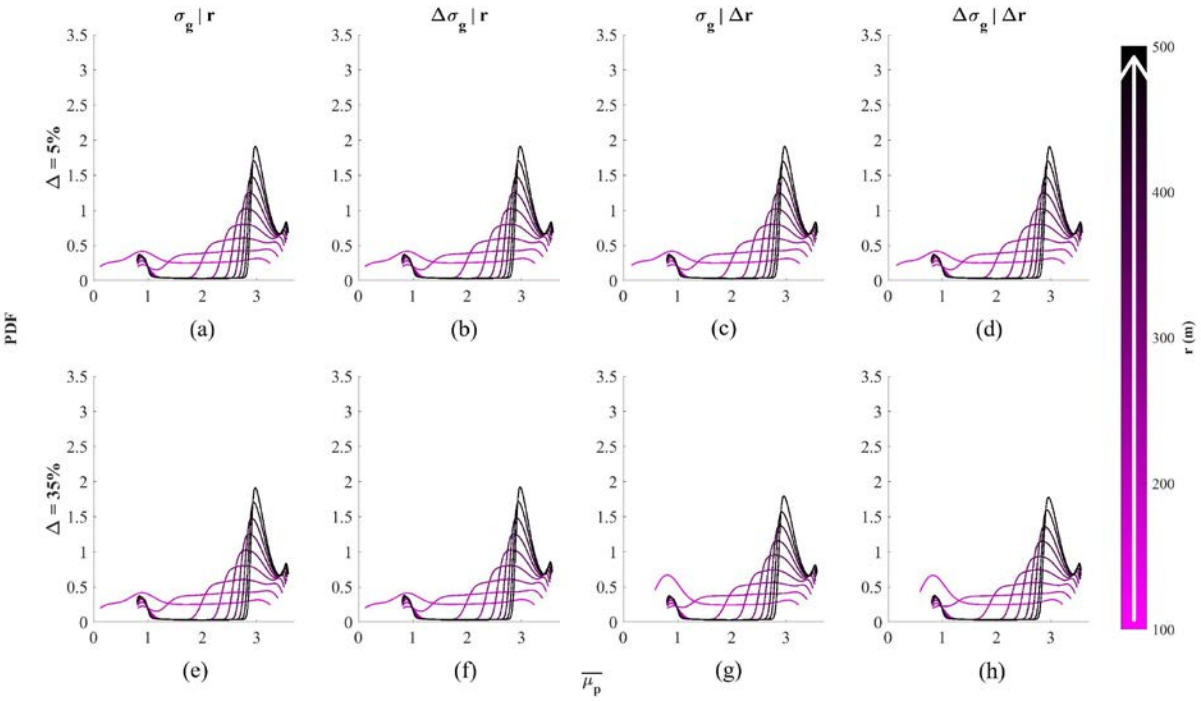

Figure 6: PDFs for the average ratio of the sound pressure amplitudes $(\overline{\mu_p})$, for an acoustically hard ground $(\sigma_g = 2000\text{kPasm}^{-2})$, where each column defining the uncertainty present and range (r) is mapped to colour, from magenta $(100m)$ to black $(500m)$. Uncertainty (Δ) is at 5% in the first row and increased to 35% in the second row.

It is apparent that a PDF of the average ratio of the sound pressure amplitudes $(\overline{\mu_p})$ is not generally affected by smaller uncertainties or effective flow resistivity (σ_g). This mirrors the behaviours seen in a similar study into excess attenuation [7]. The range (r) and frequency (ω) shape the spectrum and PDF behaviours, with the range (r) being the dominant parameter which effect becomes more pronounced as the uncertainty increases.

3.2. Phase difference

Similar to the procedure reported in Section 3.1 the behaviour of the average phase difference spectra is studied over the four conditions: (i) the fixed values of the parameters ($\sigma_g|r$); (ii) uncertain value of the effective flow resistivity ($\Delta\sigma_g|r$); (iii) uncertain value of the range ($\sigma_g|\Delta r$); and (iv) uncertain values of the effective flow resistivity and range ($\Delta\sigma_g|\Delta r$). Two sets of results are presented: (i) for $\Delta = 5\%$ of the given true value ((a), (b), (c) and (d) in Fig. 5); and (ii) for $\Delta = 35\%$ of the given true value ((e), (f), (g) and (h) in Fig. 5). Fig. 6 presents a similar set of results for the case of hard ground.

The results of these simulations suggest that the variation in the average phase difference spectra $(\overline{\mu_\phi})$ for any combination of small uncertainties $(\Delta = 5\%)$ is relatively small, i.e. that this parameter predicted for the chosen microphone locations is relatively immune to the variation in the true value of the range or effective flow resistivity of the ground. The frequency (ω) is the dominant parameter here. Visually, the spectra only show discernible differences from the true spectra, irrespective of the impedance ground (σ_g) ((a) and (e) in Fig. 7 and Fig. 8), when the uncertainty in the range (r) is high $(\Delta = 35\%)$ and at shorter ranges, i.e. $r \leq 150m$.

The effect of the effective flow resistivity on the mean of the average phase difference $(\overline{\mu_\phi})$ is more significant than on the average sound pressure amplitude ratio $(\overline{\mu_p})$ (See Appendix A). The mean of $\overline{\mu_\phi}$ seen in Table 1 (See Appendix) for a soft ground $(\sigma_g = 100kPasm^{-2})$ starts at ~ 0.8 and

reduces to ~ 0.1 at the maximum range of 100m. These mean values change from 0.65 to -0.015, respectively, when the impedance of the ground hardens and the effective flow resistivity is increased to $\sigma_g = 2000kPasm^{-2}$. The standard deviation of the average absolute phase difference $(\overline{\mu_\phi})$ decreases with the increased range (r).

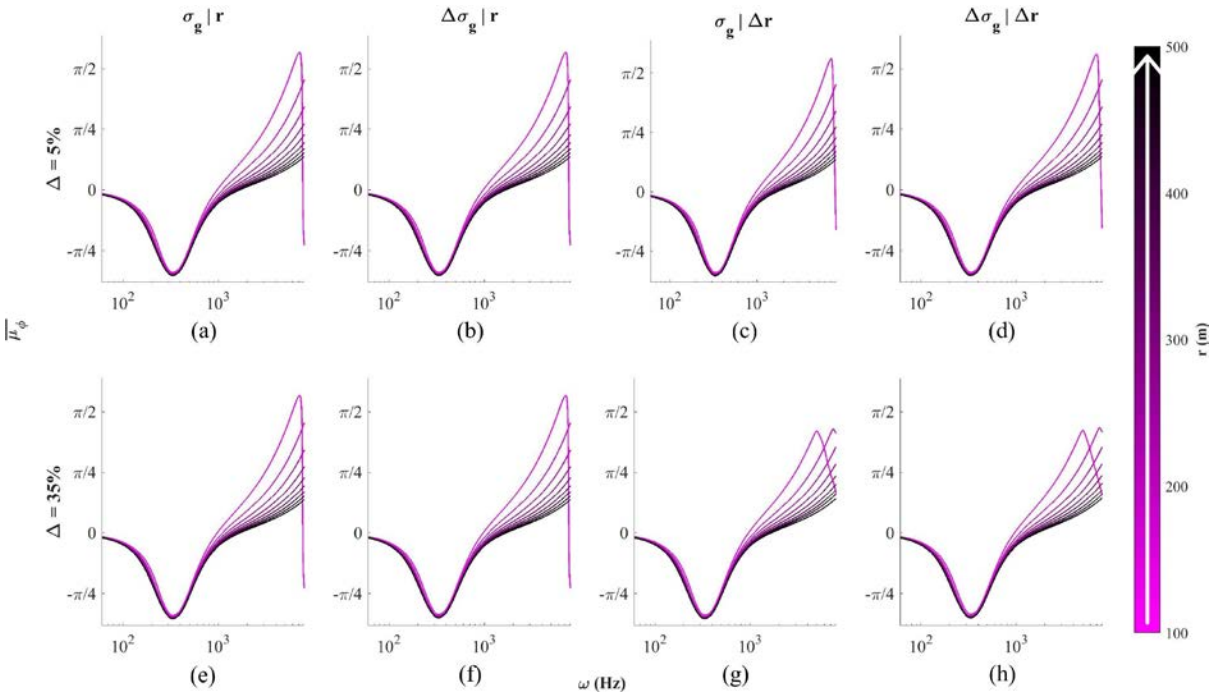

Figure 7: Simulation results for the average phase difference $(\overline{\mu_\phi})$, for an acoustically soft ground $(\sigma_g = 100\text{kPasm}^{-2})$, where each column defining the uncertainty present and range (r) is mapped to colour, from magenta $(100m)$ to black $(500m)$. Uncertainty (Δ) is at 5% in the first row and increased to 35% in the second row.

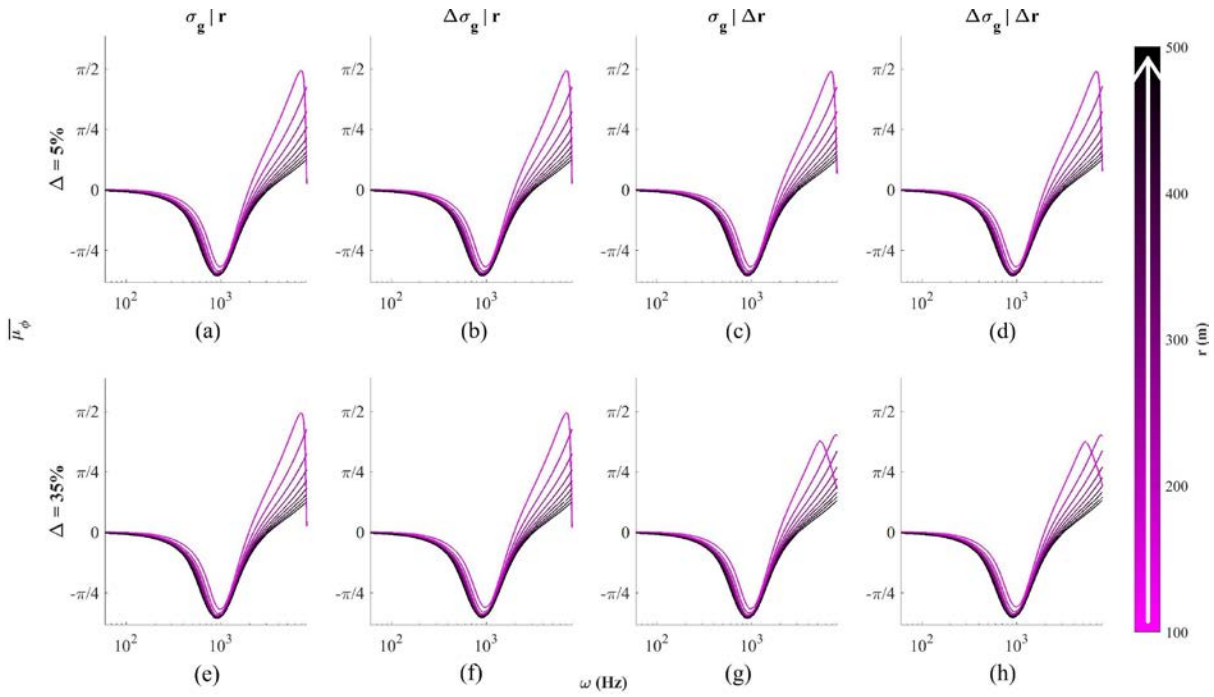

Figure 8: Simulation results for the average phase difference $(\overline{\mu_\phi})$, for an acoustically hard ground $(\sigma_g = 2000\text{kPasm}^{-2})$, where each column defining the uncertainty present and range (r) is mapped to colour, from magenta $(100m)$ to black $(500m)$. Uncertainty (Δ) is at 5% in the first row and increased to 35% in the second row.

The PDFs for the average phase difference $(\overline{\mu_\phi})$ show a different shape than that of the average absolute pressure ratio $(\overline{\mu_p})$. These PDFs depend strongly on the range (r), as the peak, and maximum attainable values for average phase difference $(\overline{\mu_\phi})$ of each simulation are directly linked to the range (r), as seen by the evolution between simulations by the colour mapping (Fig. 9 and Fig. 10). The lower values of average phase difference are not seemingly affected by the range (r). The change in the impedance ground affects the gradient of the slope of these PDFs, these data show a little ground effect even with the addition of higher uncertainty. When the range is small $(r \leq 150m)$ the PDFs for the average phase difference show a much more complex behaviour than those predicted for greater ranges ((c), (d), (g) and (h) in Fig. 9 and Fig. 10). This complex behaviour is exacerbated by an increase in uncertainty in the range parameter.

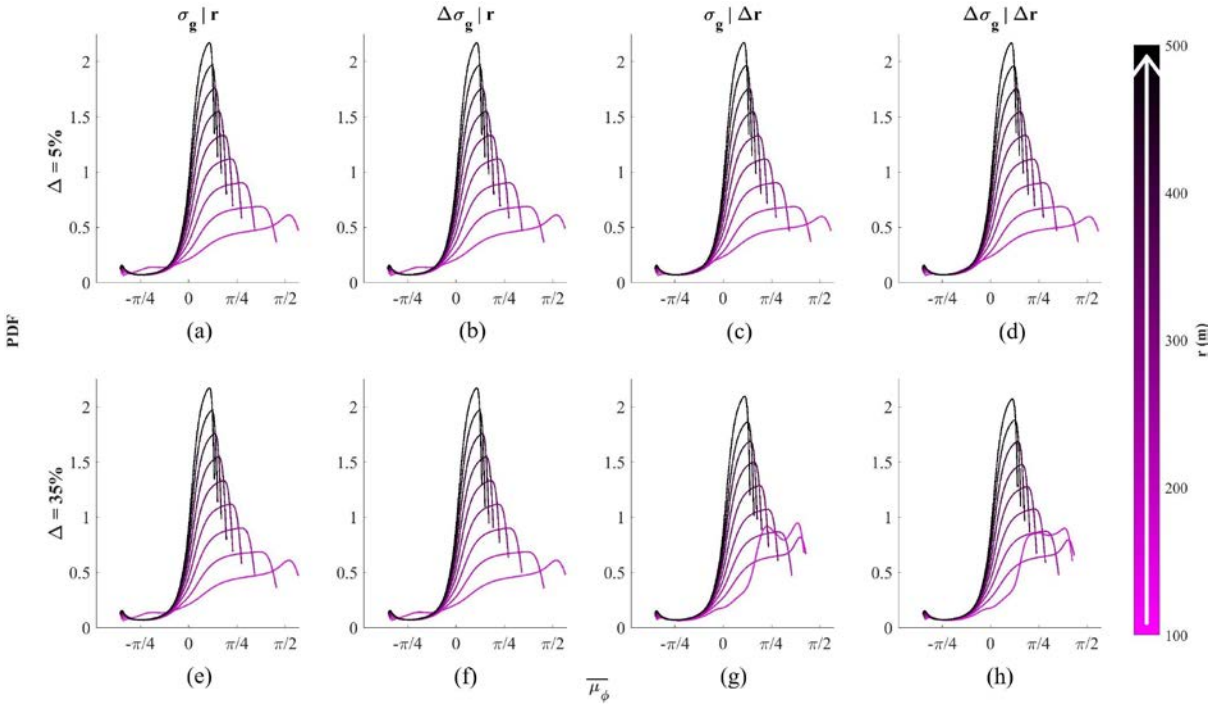

Figure 9: PDFs for the average phase difference $(\overline{\mu_\phi})$, for an acoustically soft ground $(\sigma_g = 100\text{kPasm}^{-2})$, where each column defining the uncertainty present and range (r) is mapped to colour, from magenta $(100m)$ to black $(500m)$. Uncertainty (Δ) is at 5% in the first row and increased to 35% in the second row.

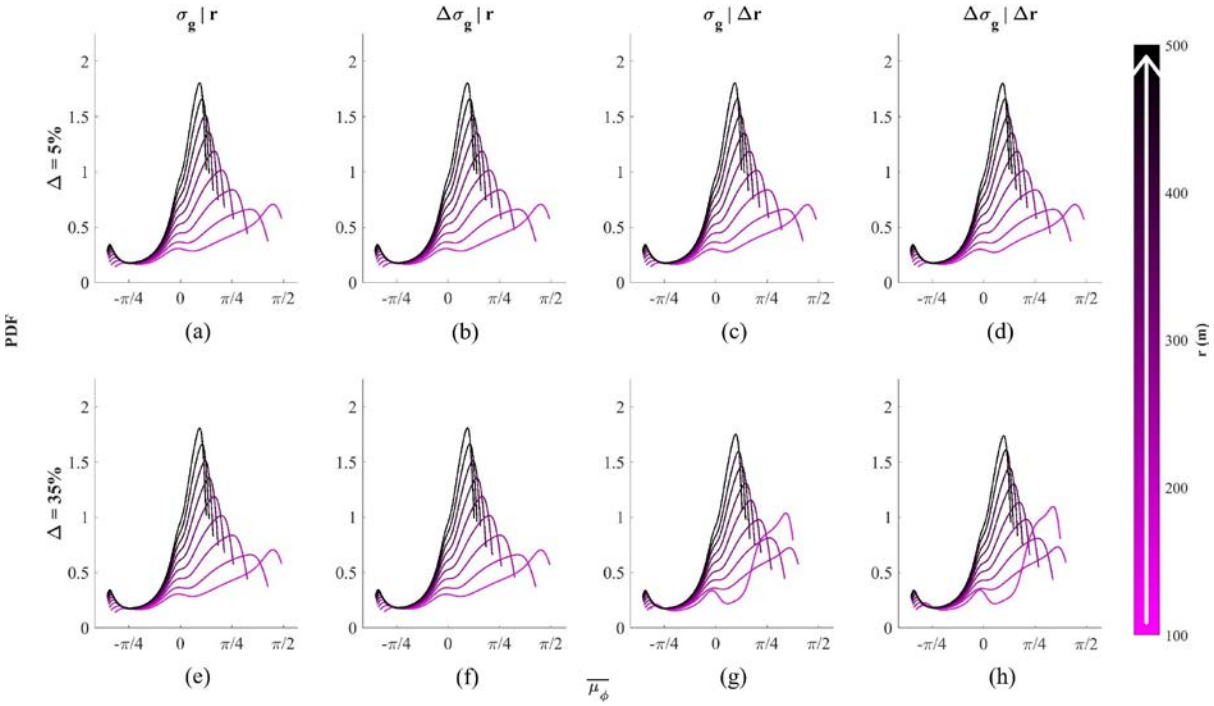

Figure 10: PDFs for average phase difference $(\overline{\mu_\phi})$, for an acoustically hard ground $(\sigma_g = 2000\text{kPasm}^{-2})$, where each column defining the uncertainty present and range (r) is mapped to colour, from magenta $(100m)$ to black $(500m)$. Uncertainty (Δ) is at 5% in the first row and increased to 35% in the second row.

It is apparent that like in the case of the average absolute pressure ratio $(\overline{\mu_p})$, the PDFs for average phase difference $(\overline{\mu_\phi})$ are not influenced significantly by smaller uncertainties. An increase in the ground impedance reduces the peak in the PDF for the average phase difference at longer ranges, but it does not change the value at which this peak actually occurs. The range and frequency control the PDFs. The range is the most influential parameter, which can be useful for source localisation applications.

4. Conclusions

The two-microphone method is found to be suitable for the characterisation of sound pressure and related measurements. This is said to be true within favourable atmospheric conditions, although the authors suggest that this conclusion needs testing in the presence of realistic atmospheric effects such as sound speed gradient and turbulence. The use of the two-microphone method can be helpful in applications related to source localisation and when the range is greater than $100 - 150m$, because the simulations show that this method can be less consistent over the shorter ranges and higher uncertainties. This method seems much more immune to the uncertainties in the range and ground impedance than alternative methods based on single microphone data, e.g. that reported in ref. [7].

The results suggest that the uncertainty in the ground does not seem to be significant unless the it is relatively high (e.g. $\Delta = 35\%$) and the range is relatively short (e.g. $r \leq 150m$). In this case, the uncertainty in the range has the dominant effect of the sound pressure ratio spectra and resultant PDFs. Combination of uncertainties in the ground impedance and range results in an increased variability in the predictions of the sound pressure ratio between two microphone positions. This suggests that for applications of the two-microphone method: (i) removal of uncertainty in the range is key for reliably source localisation/inferences, particularly at shorter distances $(r < 150)$; and (ii) uncertainty in the effective flow resistivity of the ground is unlikely to affect the behaviour of the PDF

for the sound pressure ratio, but relaxing this parameter would result in reduced computational costs with negligible, if any, loss in accuracy.

The frequency has a strong effect on stability of the two-microphone method. For frequencies below $100Hz$ the absolute pressure ratio is close to unity and phase difference is close to zero. This small difference between the two sound pressures in this frequency range is likely to affect the quality of inference if this method applied to sources which frequency spectrum is dominated by low frequency components, e.g. gun fire. Larger separations between the two microphones which are comparable with the paths difference and wavelength may be required to enhance the sensitivity of the two-microphone method for applications in this frequency range.

Acknowledgements

The author/s acknowledge the support of Defense Science and Technology Laboratory (Dstl) UK and EPSRC CASE studentship award to the University of Sheffield.

References

[1] J. M. Sabatier, R. Raspet, and C. K. Frederickson, “An improved procedure for the determination of ground parameters using level difference measurements,” J. Acoust. Soc. Am., 94(1), 396–399. (1993)

[2] G. A. Faranosov, I. V. Belyaev, V. F. Kopiev, M. Y. Zaytsev, A. A. Aleksentsev, Y.V. Bersenev, V. A. Chursin and T. A. Viskova, “Adaptation of the azimuthal decomposition technique to jet noise measurements in full-scale tests,” AIAAJ, 55(2), 572–584. (2017)

[3] Y. Hosokawa,Y. Hirano, D. Kominami, I. Aihara and M. Murata, “Implementation of a real-time sound source localization method for outdoor animal detection using wireless sensor networks,” Proceedings of the 13th International Conference on Signal Processing and Communication Systems. (Gold Coast, 2019)

[4] American National Standard – Method for Determining the Acoustic Impedance of Ground Surfaces, ANSI/ASA S1.18, 2018

[5] D. C. Hothersall and J. N. B. Harriott. “Approximate models for sound propagation above multi-impedance plane boundaries”, J. Acoust. Soc. Am., 97(2), 918-926. (Feb 1995).

[6] R. Kruse and V. Mellert. “Effect and minimization of errors in in situ ground impedance measurements”, Applied Acoustics, 69(10), 884-890. (October 2008).

[7] J. A. Parry, K. V. Horoshenkov and D. P. Williams. “Investigating Uncertain Geometries Effect on Sound Propagation in a Homogeneous and Non-Moving Atmosphere over an Impedance Ground.” Applied Acoustics, 160. (March 2020)

[8] E.M. Salomons. Computational Atmospheric Acoustics, Kluwer Academic Publishers. (2001)

[9] O. Dazel, J.P. Groby and K.V. Horoshenkov. ‘Asymptotic limits of some models for sound propagation in porous media and the assignment of the pore characteristic lengths’, J. Acoust. Soc. Am., 139(5), 2463-2474. (May 2016).

[10] K. Attenborough. “Outdoor ground impedance models”. J. Acoust. Soc. Am., 129(50), 2806–19. (May 2011)

Appendix A. Table of Statistics

		Average absolute pressure $(\overline{\mu_p})$				Average phase difference $(\overline{\mu_\phi})$			
		Mean (μ)		Std. Dev. (σ)		Mean (μ)		Std. Dev. (σ)	
$\sigma_g\ (kPasm^{-2})$	$r\ (m)$	$\Delta = 5\%$	$\Delta = 35\%$	$\Delta = 5\%$	$\Delta = 35\%$	$\Delta = 5\%$	$\Delta = 35\%$	$\Delta = 5\%$	$\Delta = 35\%$
100	100	1.7279		1.037		0.8282		0.7405	
	150	2.3467		0.6615		0.6182		0.5696	
	200	2.6156		0.5134		0.4401		0.4731	
	250	2.7505		0.4573		0.3322		0.4157	
	300	2.8269		0.4344		0.2599		0.3782	
	350	2.8743		0.4242		0.2082		0.3518	
	400	2.9057		0.4193		0.1693		0.3324	
	450	2.9275		0.4167		0.1391		0.3176	
	500	2.9434		0.4154		0.1148		0.3059	
	Δ100	1.7302	1.7568	1.0328	0.927	0.8267	0.6842	0.7028	0.5339
	Δ150	2.3445	2.2881	0.6628	0.6916	0.6194	0.6367	0.5702	0.5732
	Δ200	2.6516	2.5701	0.5134	0.5345	0.44	0.4638	0.473	0.4857
	Δ250	2.7499	2.7185	0.4575	0.4686	0.3325	0.3515	0.4159	0.4259
	Δ300	2.8257	2.8061	0.4347	0.4398	0.261	0.2737	0.3787	0.3852
	Δ350	2.874	2.8607	0.4242	0.4268	0.2085	0.2179	0.352	0.3567
	Δ400	2.9056	2.8923	0.4193	0.4212	0.1694	0.1809	0.3325	0.3382
	Δ450	2.9274	2.9141	0.4167	0.4182	0.1392	0.1529	0.3177	0.3243
	Δ500	2.9434	2.9532	0.4154	0.416	0.1148	0.1231	0.3059	0.3099
Δ100	100	1.7279	1.7277	1.037	1.0356	0.8282	0.8287	0.7404	0.7394
	150	2.3467	2.3464	0.6615	0.6591	0.6182	0.6188	0.5696	0.5684
	200	2.6156	2.6153	0.5133	0.5102	0.4401	0.4406	0.4731	0.4718
	250	2.7505	2.7502	0.4572	0.4537	0.3322	0.3327	0.4157	0.4144
	300	2.8269	2.8267	0.4343	0.4306	0.2599	0.2604	0.3781	0.3768
	350	2.8943	2.8741	0.4241	0.4203	0.2082	0.2087	0.3518	0.3505
	400	2.9057	2.9054	0.4192	0.4153	0.1693	0.1698	0.3324	0.331
	450	2.9275	2.9273	0.4167	0.4128	0.1391	0.1396	0.3176	0.3162
	500	2.9434	2.9431	0.4153	0.4114	0.1148	0.1153	0.3059	0.3045
	Δ100	1.7288	1.7475	1.033	0.9282	0.8251	0.6825	0.7014	0.5324
	Δ150	2.345	2.2825	0.6624	0.6933	0.6191	0.6417	0.57	0.5755
	Δ200	2.6149	2.5759	0.5137	0.529	0.4404	0.46	0.4733	0.4825
	Δ250	2.7497	2.7192	0.4575	0.4653	0.3327	0.3512	0.416	0.4245
	Δ300	2.8268	2.8031	0.4344	0.4374	0.2599	0.2769	0.3781	0.3857
	Δ350	2.8742	2.8552	0.4242	0.4246	0.2082	0.2239	0.3518	0.3585
	Δ400	2.9054	2.8918	0.4193	0.418	0.1696	0.1814	0.3326	0.3372
	Δ450	2.9272	2.9157	0.4167	0.4147	0.1395	0.1508	0.3178	0.322
	Δ500	2.9431	2.9329	0.4154	0.4129	0.1152	0.1263	0.3061	0.3101
2000	100	1.6702		0.9787		0.6473		0.7462	
	150	2.2784		0.7535		0.4345		0.6579	
	200	2.5488		0.704		0.2713		0.569	
	250	2.6876		0.6994		0.1703		0.5146	
	300	2.7678		0.7034		0.102		0.4785	
	350	2.8185		0.7083		0.0528		0.4528	
	400	2.8527		0.7125		0.0158		0.4337	
	450	2.877		0.7159		-0.0131		0.4189	
	500	2.8948		0.7185		-0.0364		0.4072	
	Δ100	1.6706	1.6846	0.9761	0.8852	0.6399	0.5111	0.7389	0.6153
	Δ150	2.2779	2.2306	0.7536	0.7632	0.4346	0.4458	0.6579	0.6591
	Δ200	2.549	2.5052	0.704	0.7078	0.271	0.2918	0.5688	0.5799
	Δ250	2.6867	2.6548	0.6994	0.6989	0.1708	0.1886	0.5149	0.5243
	Δ300	2.7677	2.748	0.7034	0.7018	0.102	0.1139	0.4785	0.4847
	Δ350	2.8181	2.8009	0.7083	0.7063	0.0532	0.0654	0.453	0.4593
	Δ400	2.8529	2.8391	0.7125	0.7106	0.0156	0.0264	0.4336	0.4391
	Δ450	2.8765	2.8637	0.7158	0.7138	-0.0126	-0.0011	0.4192	0.425
	Δ500	2.8948	2.8859	0.7185	0.717	-0.0364	-0.0283	0.4072	0.4112
Δ2000	100	1.6702	1.671	0.9786	0.9758	0.6473	0.6494	0.7462	0.7447
	150	2.2784	2.2793	0.7534	0.7481	0.4345	0.4366	0.6579	0.6559
	200	2.5488	2.5497	0.7039	0.6975	0.2712	0.2732	0.5689	0.5668
	250	2.6876	2.6884	0.6993	0.6926	0.1702	0.1721	0.5146	0.5123
	300	2.7678	2.7686	0.7033	0.6965	0.102	0.1038	0.4784	0.4761
	350	2.8185	2.8193	0.7082	0.7014	0.0528	0.0546	0.4528	0.4504
	400	2.8527	2.8534	0.7125	0.7056	0.0158	0.0175	0.4337	0.4313
	450	2.877	2.8776	0.7158	0.7089	-0.0132	-0.0114	0.4189	0.4165
	500	2.8948	2.8955	0.7184	0.7116	-0.0364	-0.0346	0.4072	0.4048
	Δ100	1.6727	1.695	0.9753	0.8778	0.6405	0.5138	0.739	0.6137
	Δ150	2.2766	2.2218	0.7538	0.761	0.4352	0.4497	0.6583	0.6588
	Δ200	2.5479	2.5014	0.704	0.7034	0.2716	0.2942	0.5692	0.5794
	Δ250	2.6872	2.6551	0.6993	0.6942	0.1704	0.1881	0.5147	0.5222
	Δ300	2.7676	2.7397	0.7034	0.6967	0.102	0.1209	0.4785	0.4865
	Δ350	2.8184	2.7992	0.7083	0.7016	0.0528	0.0667	0.4528	0.4581
	Δ400	2.8523	2.8362	0.7124	0.7059	0.0161	0.0294	0.4338	0.4388
	Δ450	2.8769	2.8661	0.7158	0.7099	-0.0132	-0.0039	0.4189	0.4217
	Δ500	2.8945	2.8839	0.7184	0.7125	-0.036	-0.0258	0.4074	0.4106

Table 1: Table of means (μ) and std. deviations (σ) for simulation results for average absolute pressure ratio $(\overline{\mu_p})$ and average phase difference $(\overline{\mu_\phi})$ at each combination of given parameters and uncertainty (Δ).